ARTICLE   OPEN

Check for updates

Specific behavior of transition metal chloride complexes for achieving giant ionic thermoelectric properties

Bin Chen[1], Jiansong Feng[1], Qianling Chen[1], Songhua Xiao[1], Jing Yang[1], Xu Zhang[1], Zhibin Li[1] and Taihong Wang [1]✉

When people are keen to exploring the thermoelectric properties of polymer composite inorganic electrolyte aqueous flexible electronic devices, the complicated chemical configuration of transition metal chloride anion has not been paid attention and reported. Here, we demonstrate a hydrated polyvinyl alcohol (PVA)-cellulosic membrane that relies on the thermal gradient diffusion of transition metal and chloride complexe $[CuCl_4]^{2-}$ enhanced by copper-coordinated carboxylated cellulose. The PVA-cellulosic membrane exhibits a thermopower of -26.25 mV·K^{-1}, rendering it among the best n-type ionic thermoelectric materials under the same conditions. We attribute the enhanced thermally generated voltage to the highly-coordinated configuration of Cu^{2+} - Cl^-, which converts the independent thermal motion of Cu^{2+} and $Cl-$ to the higher ion transport heat of $[CuCl_4]^{2-}$ anion via carboxylated cellulose, while this phenomenon do not occur in the other transition metal chlorides. This specific heat transport behavior of $[CuCl_4]^{2-}$ has important implications in designing high-quality ionic thermoelectric materials.

INTRODUCTION

Since the 21st century, with the popularity and rapid development of wearable devices, providing sustainable thermal conversion energy for the wearable devices has become a hot research topic in the world[1–7]. Traditional semiconductor electronic thermo-electric devices are widely used in the thermal energy harvesting at medium and high temperature[8,9]. However, for the low-grade thermal energy harvesting (the heat source temperature <100 °C), especially in the field of self-functioning wearable thermoelectric devices, the lower thermal response voltage under per unit temperature of semiconductor thermoelectric devices and their rigid physical properties usually lead to the results that they are difficult to be applied flexibly. Emerging in 2010, a new type of ionic thermoelectric device based on the Soret effect can generate the voltage response of mV·K^{-1} in a limited temperature range, and also has low thermal conductivity and higher mechanical flexibility, so it has become one of the most competitive candidates to provide thermal conversion energy for wearable devices[10–14].

In the typical polar aqueous solution, the Agar model based on the Born theory using standard ion transport heat ($Q^{*\underline{Q}}$) is often used to estimate the thermopower of inorganic electrolytes[15–17]. $Q^{*\underline{Q}}$ is related to the interaction among the ions and that between ions and solvent molecules[18]. But, due to the hydration interaction of ions, the intrinsic Coulomb interaction between anions and cations is shielded, corresponding to thermopower <1 mV·K^{-1} [19]. Recent studies have shown that the rational application of ion-polymer interaction in ionic aqueous solutions is an effective way to achieve high-quality thermopower. Specifically, the efficient inter-calation of sodium ions in oxidized cellulose nanochannels obtained the thermopowers as high as $+24$ mV·K^{-1} [20]. The gelatin matrix modulated with KCl-[K$_4$Fe(CN)$_6$/K$_3$Fe(CN)$_6$] as the ion provider proofed a huge positive thermopower of $+17.0$ mV·K^{-1} [21]. In the electronic and ionic mixed systems, bidirectionally tunable thermo-powers of $+16.2$ and -18.2 mV·K^{-1} were recorded using poly(3,4-ethylene-dioxythiophene)-poly(styrene sulfonate) and HCl/CuCl$_2$, respectively[22,23]. The physical core of this methods can be attributed

to the contribution of the enhanced ion transport heat to the thermal response voltage. Because another contributing factor to the high $Q^{*\underline{Q}}$ value is the widespread coordination/dipole interac-tions between ions and polymers.

However, it is worth noting that the complex chemical configuration of transition metal chlorides is easily overlooked when people explore the thermoelectric properties of polymer composite inorganic electrolyte aqueous solutions. Extensive molecular dynamics simulations have pointed to the existence of extensive and stable transition metal chloride complexes in the aqueous solutions[24,25]. Particularly impressive, some reports even showed that the complex $[CuCl_4]^{2-}$ of Cu^{2+} and Cl^- had a weaker hydration interaction than that of Cu^{2+} (Fig. 1a)[26]. This endows $[CuCl_4]^{2-}$ with a faster diffusion rate and a larger heat of ion transport in the aqueous solution, which is a key signal for the study of n-type ionic thermoelectric materials. Because the core of ionic thermoelectric performance lies in the differential ion transport heat between anions and cations. In addition, the application of transition metal-chloride complexes, for the thermoelectric Agar model of Born theory, this is also no longer only considering the coupling of a single ion to the thermal field. Furthermore, the high concentration of chloride environment is a favorable condition to promote the formation of $[CuCl_4]^{2-}$. But, in the field of ionic thermoelectrics, high-concentration electrolytes normally mean low-response thermopower. How to generate more $[CuCl_4]^{2-}$ under limited electrolyte concentration is the central problem that we need to solve. Carboxylated cellulose is rich in oxygen-containing functional groups and COO$^-$ ions, and the affinity of Cu^{2+} to cellulose is a well-known phenomenon for dissolving cellulose and forming permanent Cu^{2+}-cellulose coordination structures[27–29]. We guess that relying on the affinity between Cu^{2+} and carboxylated cellulose to achieve an enriched environment for chloride ions, further inducing more $[CuCl_4]^{2-}$ formation, is more likely to be the solution to the problem (Fig. 1b). In a word, we speculate that synthetic $[CuCl_4]^{2-}$ induced by carboxylated cellulose in CuCl$_2$ aqueous solution may have a

[1]Department of Electrical and Electronic Engineering, Southern University of Science and Technology, Shenzhen, Guangdong 518055, China. ✉email: wangth@sustech.edu.cn
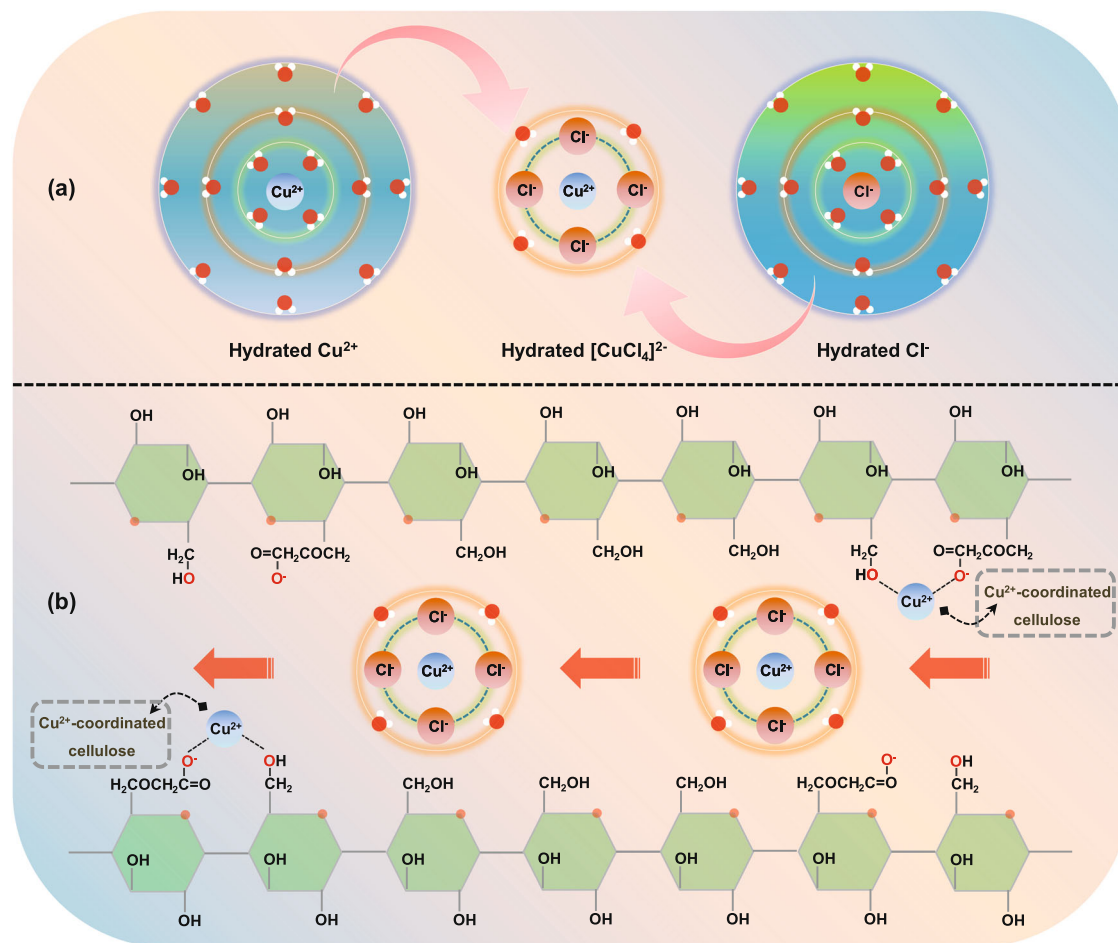
Fig. 1 Design principle for copper-coordinated cellulose ionic conductors. a Chemical configuration of hydrated ions (Cu^{2+}, Cl^- and $[CuCl_4]^{2-}$). **b** Synthesis of $[CuCl_4]^{2-}$ enhanced by carboxylated cellulose in $CuCl_2$ aqueous solution. Photo credit: Bin Chen, Department of Electrical and Electronic Engineering, Southern University of Science and Technology.

higher ion transport heat than Cu^{2+}, thereby achieving high-quality n-type ionic thermoelectric performance.

In this research, we explored the synthetic strategy of polymer-enhanced transition metal chloride complexes ($[CuCl_4]^{2-}$). This strategy was based on the coordinative coupling between Cu^{2+} and carboxylated cellulose polymer segments, which facilitated the generation of $[CuCl_4]^{2-}$ and the selective thermal diffusion of anions. We first dissolved the $CuCl_2$ electrolyte in a polyethylene glycol (PEO20K) aqueous solution. Then, the $CuCl_2$-PEO aqueous solution was fully penetrated into the PVA-carboxylated cellulose dry film. The synergistic coordination of PEO with high Gutmann donor number and polyanionic electrolyte cellulose to Cu^{2+} successfully achieves a huge negative thermoelectric potential (-26.25 mV·K^{-1}) and higher ionic conductivity (8.47 mS·cm^{-1}) as an ionic conductor. We envision this ion-selective cellulose membrane for a range of potential applications, including the design of ultrasensitive ion thermopiles and low-grade thermal energy harvesting.

RESULTS AND DISCUSSION
Material characterization
We chose PEO and carboxylated cellulose to jointly enhance the coordination interaction between Cu^{2+} and polymer. Although, molecular dynamics simulations of solid-state electrolytes have pointed out that Lewis basic polymers (PEO) have stronger coordination interactions with cationic groups[30]. But it seems

more reasonable to use Gutmann donor rule to initially analyze the interaction between PEO and Cu^{2+} in aqueous solution[31]. The monomer chemical structure of PEO can be regarded as a composite configuration composed of Ethanediol (DN = 20.0 kcal·mol^{-1}), Diethylether (DN = 19.2 kcal·mol^{-1}) and 1,2-Dimethoxyethane (DN = 24.0 kcal·mol^{-1}) (Fig. 2a)[32,33]. The Gutmann DN of PEO monomer is about 19.2–24 kcal·mol^{-1}, while the Gutmann DN of H_2O is 18.0 kcal·mol^{-1}. Clearly, Cu^{2+} tends to have a stronger coordination interaction with PEO. The coordination interaction of cellulose-Cu^{2+} depends on the charge density of cellulose, that is, the degree of carboxylation (-COO$^-$). Utilizing freeze-drying technology, our prepared PVA-carboxylated cellulose dry film has large-area production and flexible operability. Finally, we constructed the thermoelectric ionic conductors by infiltrating PVA-cellulosic membranes with $CuCl_2$-PEO-based polymer aqueous electrolytes and applying a temperature difference across the membranes.

The huge ratio of hydroxyl and carboxyl groups on the cellulose molecular chain endows it with negative charges, which can be confirmed by the zeta potential of -22 mV in cellulose aqueous solution (Fig. 2b)[34]. Using dynamic light scattering (DLS) to measure the hydrodynamic radius (Rh) of diluted cellulose and PEO aqueous solutions[35], we determined the strength of the coordination interaction between Cu^{2+} with PEO and cellulose, respectively (Fig. 2c). Nanoparticles with a particle size of ~500 nm in both $CuCl_2$-PEO and $CuCl_2$-cellulose increased in size to large agglomerates as the Cu^{2+} concentration increased. Moreover, the coordination interaction between Cu^{2+} and negatively charged cellulose is significantly
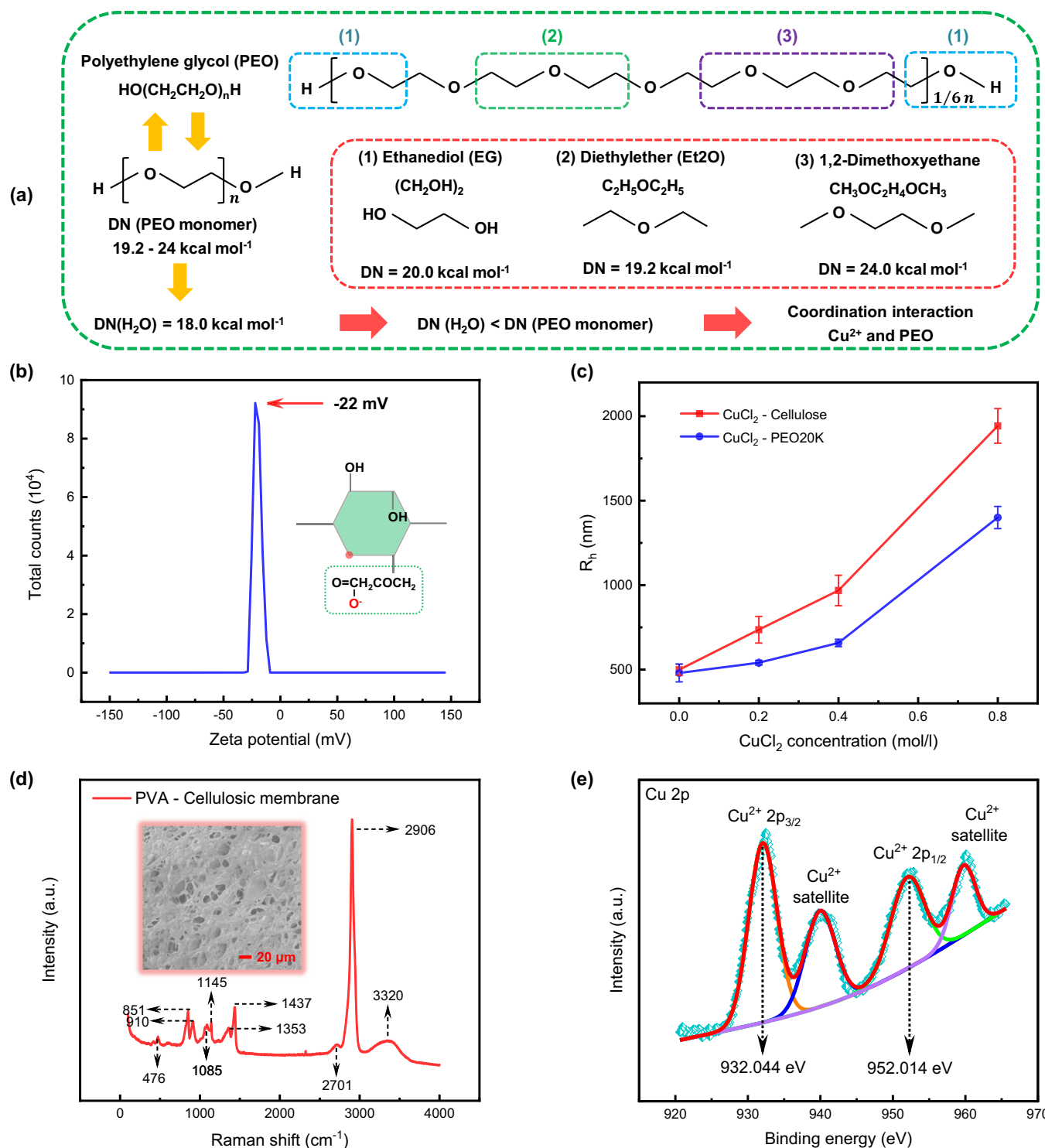
Fig. 2 Characterization of the PVA-cellulosic membrane. a PEO-Cu^{2+} coordination interaction based on Gutmann's donor rule in aqueous solution. **b** Zeta potential of the cellulose aqueous solution. **c** Hydrodynamic radius of diluted $CuCl_2$-cellulose and $CuCl_2$-PEO aqueous solutions. **d** Raman peak of the PVA-cellulosic membrane. The inset was the SEM image of the PVA-cellulosic membrane. **e** High-resolution Cu 2p photoelectron spectra of the $CuCl_2$ - [PVA-cellulosic membrane].

stronger. Considering the low solid content and high viscosity of cellulosic aqueous solutions, it was necessary to prepare the porous PVA-cellulose dry templates (2 mm-thick) by freeze-drying in the design of the synergistically enhanced Cu^{2+} coordination by PEO and cellulose. In addition, the Coulomb repulsive force between COO^- functional groups in the cellulose chain is also the main consideration for using PVA as a cellulose gel matrix. Specifically, Raman

spectroscopy was used to analyze the crystallinity of the PVA gel matrix in the cellulose dry film (Fig. 2d)[36,37]. 1142 cm^{-1} is the fingerprint peak of PVA crystallinity. It is the C-C stretching vibration peak related to the C-O stretching vibration, that is, the symmetrical stretching vibration peak of O-C-C. Moreover, the pore size of the PVA-cellulosic membrane was about 10–20 μm (inset of Fig. 2d and Supplementary Fig. 1). This provided the necessary conditions for the

penetration of the CuCl₂-PEO aqueous solution. From the X-ray photoelectron spectroscopy (XPS) for PVA-cellulosic membrane, two Cu 2p standard reference peaks were observed at 932.7 eV ($2p_{3/2}$) and 953.0 eV ($2p_{1/2}$) (Fig. 2e)[23,28]. The Cu 2p spectrum also showed characteristic shake-up satellites peaks. The electron binding energies of Cu 2p core levels were all slightly lower than their reference values, which was mainly due to the coordination of oxygen atoms on -OH/COO⁻ (Cellulose) with metal ions (Cu^{2+}), resulting in the electron cloud density of metal ions increasing, the shielding effect was enhanced, and the electron binding energy at the core level decreased. Meanwhile, the coordination interaction between PEO and Cu^{2+} can also cause the movement of Cu 2p peaks to the short wavelength direction (Cu^{2+} $2p_{3/2}$ = 932.680 eV; Cu^{2+} $2p_{1/2}$ = 952.456 eV) (Supplementary Fig. 2). But its movement amplitude was significantly weaker than that of PVA-cellulosic membrane (Cu^{2+} $2p_{3/2}$ = 932.044 eV; Cu^{2+} $2p_{1/2}$ = 952.014 eV). This proved that the PVA-cellulosic membrane played a major role in the synergistic coordination of Cu^{2+} by the PVA-cellulosic membrane and PEO.

The color of Cu^{2+} in aqueous solution is blue and the color of $[CuCl_4]^{2-}$ is yellow, so the color of the mixed solution of Cu^{2+} and $[CuCl_4]^{2-}$ should be green. The distinct green color existed at the bottom of the unstirred aqueous CuCl₂ solution, which was the most direct experimental evidence for the presence of $[CuCl_4]^{2-}$ in the aqueous solutions (Supplementary Fig. 3a). Although, after being fully stirred, the color of the CuCl₂ aqueous solutions completely changed to blue (Fig. 3a). In particular, after adding PEO to the blue CuCl₂ aqueous solutions with different concentrations, the re-emergence of green color and the gradual deepening of the color can be clearly observed. This was consistent with our original experimental design. In other words, the coordination interaction between PEO and carboxylated cellulose with Cu^{2+} promoted the transformation of independent Cu^{2+} and Cl⁻ thermal motions into mobile $[CuCl_4]^{2-}$. We also performed colorimetric experiments on the thermal response behavior of CuCl₂ aqueous solution and CuCl₂-PEO aqueous solution. The experimental results showed that the increase of temperature facilitated the synthesis of $[CuCl_4]^{2-}$ and this behavior was reversible. This thermally responsive behavior, that we called 'thermosensitive coordination', which synthesized the thermosensitive $[CuCl_4]^{2-}$-coordination ions at the hot end as the temperature increased[38]. The dynamic synthesis of $[CuCl_4]^{2-}$ led to an increase in the anion concentration at the hot end, accompanied by the diffusion of $[CuCl_4]^{2-}$ towards the cold end caused by the concentration difference at the same time. This had a certain promoting effect on the thermoelectric potential of n-type ions.

To demonstrate the transport concept of $[CuCl_4]^{2-}$ anions in the dielectric, we examined its thermoresponsive voltage at different temperature gradients to obtain the thermopower of cellulose ionic conductor. The polymer dielectric used to infiltrate the PVA-cellulosic membrane was prepared from the same concentrations of PEO (35 wt%), deionized water (65 wt%) and 0.4 mol/L CuCl₂ (Fig. 3b). The use of inert Pt electrodes to prevent interfacial reactions and monitoring the temperature of both the hot and cold sides simultaneously allowed us to evaluate the response voltage due to the ion redistribution in the dielectric (Supplementary Figs. 4 and 5). First, we tested the thermopower of the classical NaOH-PEO electrolyte infiltrated PVA-cellulosic membrane. It exhibited a thermopower of +12.389 mV·K⁻¹ (Supplementary Fig. 6a), which was consistent with the literature report[20]. Next, the theoretical thermopower of CuCl₂ aqueous solution estimated by the Agar model based on Born theory was 0.153 mV·K⁻¹ (Supplementary Table 1). But our practical measured value was −0.720 mV·K⁻¹ (Supplementary Fig. 7). Referring to the theoretical thermopower (0.0506 mV·K⁻¹) and the measured value (0.259 mV·K⁻¹) of NaCl aqueous solution (Supplementary Table 1 and Supplementary Fig. 6b), we had the reason to believe that the presence of $[CuCl_4]^{2-}$ in the CuCl₂ aqueous solution contributed

to the thermopower exceeding the coupling of independent Cu^{2+} and Cl⁻ with the thermal field. And the Cl⁻ adsorption characteristic contributed by the work function of the Pt electrode was likely to enhance the measured value of NaCl aqueous solution[39,40]. Furthermore, the CuCl₂-PEO aqueous solution and the polymer-infiltrated PVA-cellulosic membrane exhibited thermopowers of −4.617 mV·K⁻¹ and −19.305 mV·K⁻¹ (Fig. 3c), respectively. This reflected the dominant role of the strong coordination interaction between CuCl₂ and the PVA-cellulosic membrane in the thermally generated voltage. The thermopower measurement of polymer-infiltrated pure PVA membrane (−5.243 mV·K⁻¹) more fully reflected that PVA in the sample mainly played the role of mechanical support, while the thermoelectric functional matrix was realized by carboxylated cellulose (Supplementary Fig. 8). In sharp contrast, the thermopower of the PVA-cellulosic membrane infiltrated by the NaCl-PEO electrolyte was 9.975 mV·K⁻¹ (Supplementary Fig. 6c), and the coordination configuration of Na⁺ and Cl⁻ did not exist in the NaCl solution.

On the other hand, the comparative analysis of the thermoelectric properties for PVA-cellulosic membrane (without COO⁻ group) and PVA-carboxylated cellulosic membrane is undoubtedly important to prove the role of the coordination effect between COO⁻ group and Cu^{2+}. The test results showed that the thermopower of the PVA-cellulosic membrane (without COO⁻ group) was −9.953 mV·K⁻¹, and the corresponding Zeta potential of the uncarboxylated cellulose aqueous solution was −2.98 mV (Supplementary Fig. 9). Compared with the thermopower (−19.305 mV·K⁻¹) and Zeta potential (−22 mV) of the PVA-carboxylated cellulosic membrane, the strong coordination effect between the COO⁻ group and Cu^{2+} was obviously the key factor to improve the thermoelectric performance of the samples. Particularly, in order to clarify the respective contributions of PEO and cellulose to the thermopower in PVA-cellulosic membrane infiltrated with PEO aqueous solution of CuCl₂, we have also weighth the mass of PVA-cellulosic membrane before and after infiltration by CuCl₂-PEO aqueous solution. This was mainly to determine the mass distribution of PVA-cellulosic membrane, PEO and CuCl₂ aqueous solution, and then drop the corresponding proportion of CuCl₂ aqueous solution into the cellulose membrane to obtain the independent thermopower of CuCl₂-[PVA-cellulosic membrane]. The measurement results showed that the PVA-cellulosic membrane infiltrated with PEO aqueous solution of CuCl₂ contained 17.91 wt% of PVA-cellulosic membrane, 28.73 wt% of PEO and 53.36 wt% of CuCl₂ aqueous solution (Supplementary Fig. 10). Based on this, the thermopower of the tested CuCl₂-[PVA-cellulosic membrane] was −12.667 mV·K⁻¹. Referring to the thermopower of the corresponding CuCl₂-PEO aqueous solution (−4.617 mV·K⁻¹), we can confirm that the contribution of PEO and PVA-cellulosic membrane to thermopower is 26.71% and 73.29%, respectively.

Obviously, the complex ions formed by metal ions and chloride ions are not unique to copper ions. We also tested the thermopowers of PVA-cellulosic membranes infiltrated with PEO and different inorganic electrolyte aqueous solution (Fig. 3d, Supplementary Figs. 11 and 12). Except for the PVA-cellulosic membrane infiltrated by the CuCl₂ electrolyte, we were very surprised to find that all the PVA-cellulosic membrane infiltrated by the other electrolytes exhibited consistent positive thermopowers, which were in partial agreement with the agar model predicted by Born's theory (Supplementary Table 1). The stable existence of metal ion chloride complexes $[CaCl_4]^{2-}$ and $[ZnCl_4]^{2-}$ similar to $[CuCl_4]^{2-}$ in aqueous solution has been reported in some literatures[20,21]. This can be observed by Raman spectroscopy of aqueous ZnCl₂ (Supplementary Fig. 13). However, PVA-cellulosic membranes infiltrated with electrolytes such as CaCl₂ or ZnCl₂ did not exhibit a negative thermoelectric potential induced by the higher ion transport heat of $[CaCl_4]^{2-}$ or $[ZnCl_4]^{2-}$ than Ca^{2+} or Zn^{2+}. According to this phenomenon, we believe that the higher
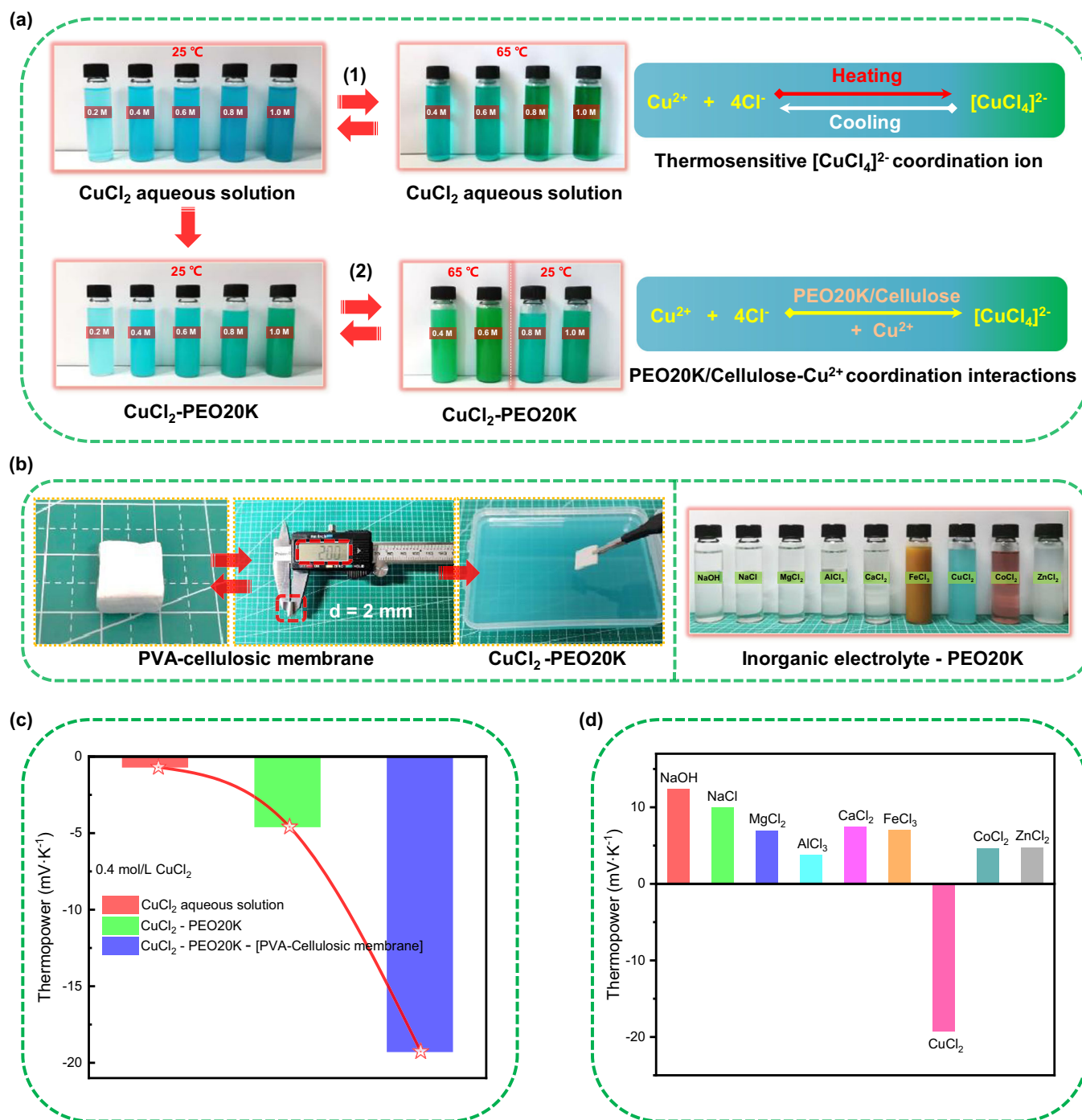
Fig. 3 Preparation process and thermoelectric properties of the PVA-cellulosic membrane. a Reversible transformation of thermosensitive coordination ion [CuCl$_4$]$^{2-}$ under the temperature gradient and the synthesis of [CuCl$_4$]$^{2-}$ enhanced by PEO-Cu^{2+} coordination interaction. **b** Preparation of polymer electrolytes and infiltration of PVA-cellulosic membranes. **c** Measured thermopowers of CuCl$_2$ aqueous solution (0.4 mol/L), CuCl$_2$-PEO aqueous solution and PVA-cellulosic membrane infiltrated with PEO aqueous solution of CuCl$_2$. **d** Measured thermopowers of PVA-cellulosic membranes infiltrated with PEO aqueous solution of different inorganic electrolyte (NaOH, NaCl, MgCl$_2$, AlCl$_3$, CaCl$_2$, FeCl$_3$, CuCl$_2$, CoCl$_2$ and ZnCl$_2$).

ion transport heat of [CuCl$_4$]$^{2-}$ than Cu^{2+} in the PVA-cellulosic membrane infiltrated by CuCl$_2$ electrolyte is the most important factor to realize the negative thermopower. The more [CuCl$_4$]$^{2-}$ synthesis caused by the coordination of PEO or cellulose with Cu^{2+} is an effective means to further amplify the negative thermopower. At present, we have not been able to give a more precise means of proving the higher ion transport heat of [CuCl$_4$]$^{2-}$ than Cu^{2+}. However, the report about aqueous solutions

of CuCl$_2$, CaCl$_2$ or ZnCl$_2$ based on molecular dynamics simulations can indirectly supplement this point[26]. They pointed out that [CuCl$_4$]$^{2-}$ had a larger diffusion coefficient than Cu^{2+}, while the diffusion coefficient of [CaCl$_4$]$^{2-}$ or [ZnCl$_4$]$^{2-}$ was smaller than that of Ca^{2+} or Zn^{2+}. Moreover, they also emphasized that the diffusion rate of metal ion chloride complexes was determined by their hydration structure. Because for symmetrical electrolyte systems ($n_0^+ = n_0^-$, [CuCl$_4$]$^{2-}$ and Cu^{2+}, [CaCl$_4$]$^{2-}$ and Ca^{2+}), the

Ion transport and regulation

Exploring the copper ion inorganic electrolytes thermoelectric properties of non-chloride ($Cu(NO_3)_2$ and $CuSO_4$) was helpful to further verify the concept of $[CuCl_4]^{2-}$ anion transport in the $CuCl_2$ aqueous solution. Both the PVA-cellulosic membranes infiltrated with PEO aqueous solution of $Cu(NO_3)_2$ and $CuSO_4$ exhibited positive thermopowers ($+4.091$ and $+2.848$ mV·K^{-1}) (Fig. 4a, Supplementary Figs. 14a and 15a). This was fundamentally different from the negative thermopower behavior of $CuCl_2$ electrolytes. Compared to chloride inorganic electrolytes, this further illustrated that the negative thermoelectric behavior was neither caused by Cu^{2+} nor Cl^- alone, but the special properties of the composite product $[CuCl_4]^{2-}$ constituted by Cu^{2+} and Cl^-. The interaction between $Cu(NO_3)_2$ or $CuSO_4$ electrolyte and polyanion electrolyte type PVA-cellulosic membrane followed Manning's counterion condensation theory (Supplementary Fig. 16)[43]. Particularly, under the temperature gradients, some of the Cu^{2+} tended to condense along the negatively charged cellulosic polymer chains and imposed frictional drags on the anions (NO_3^- or SO_4^{2-}). Cu^{2+} that was not condensed on the cellulosic chains had a faster thermophoretic mobility than anions. From another point of view, $Cu(NO_3)_2$ or $CuSO_4$ electrolyte allowed more Cu^{2+} and PEO/cellulose to form the coordinate structures, while $CuCl_2$ electrolyte was accompanied by the partial conversion of Cu^{2+} to $[CuCl_4]^{2-}$. This resulted in $Cu(NO_3)_2/CuSO_4$-cellulose having a larger hydrodynamic radius than $CuCl_2$-cellulose (Fig. 4a inset and Supplementary Fig. 17a).

The coordination configuration of Cu^{2+} and Cl^- can be easily confirmed by Raman spectroscopy of saturated $CuCl_2$ aqueous solution in the range of 200–500 cm^{-1} [24,44]. Pure water had no peaks in this range. Existing in the spectras of all copper salts, the peak around 405 cm^{-1} was assigned to $[Cu(H_2O)_x]^{2+}$ (Fig. 4b). Characteristic peaks at 290 and 245 cm^{-1} in $CuCl_2$ aqueous solution were assigned to $[Cu(H_2O)_xCl_4]^{2-}$ and $[CuCl_4]^{2-}$ (Fig. 4c). In addition, we can also observed the presence of hydrated $[CuCl_4]^{2-}$–$[Cu(H_2O)_xCl_4]^{2-}$ in the Raman spectrum of 0.4 mol/L $CuCl_2$- [PVA-cellulosic membrane] (Supplementary Fig. 17b). XPS spectra further proved the existence of $[CuCl_4]^{2-}$ (Fig. 4d). The XPS peak observed around 531.0 eV was attributed to the core level of O 1s[45]. The synthesis of $[CuCl_4]^{2-}$ led to a smaller increase in the core energy level of O 1s, compared to the $Cu(NO_3)_2$ and $CuSO_4$ electrolytes. This was consistent with the analysis of the hydrodynamic radius (Fig. 4a). It should be pointed out that the hydrolysis of Cu^{2+} may also contribute to part of the transient negative thermal response voltage. This can be more intuitively observed from the tests of $Cu(NO_3)_2$ and $CuSO_4$ aqueous solutions (Supplementary Figs. 14b and 15b). To this end, we added 0.2 mol/L HCl to the $CuCl_2$-PEO aqueous solution (pH $\approx$ 2.6) and infiltrated it into the PVA-cellulosic membrane, obtaining a comparable thermopower of -25.823 mV·K^{-1} (Supplementary Fig. 19). We also supplemented the thermally reversible color change of $CuCl_2$-PEO aqueous solution. These evidences fully demonstrated the reproducibility of both the negative thermoresponsive voltage and the $[CuCl_4]^{2-}$ reversible thermosensitive coordination phenomenon in thermoelectric material systems without the generation of permanent $Cu(OH)_2$ precipitation.

Based on the special negative thermopower of the $CuCl_2$ inorganic electrolyte, it is essential to further explore the thermoelectric properties of the similar halogen anion electrolyte $CuBr_2$. Because the reference also pointed out that transition metal and bromide complexe $[CuBr_4]^{2-}$ had similar properties to $[CuCl_4]^{2-}$ [46]. The test results showed that the PVA-cellulosic membranes infiltrated with PEO aqueous solution of $CuBr_2$ had a negative thermopower similar to that of $CuCl_2$ (Supplementary

Fig. 20). Furthermore, $CuBr_2$-PEO aqueous solution also exhibited the thermally reversible behaviour by heating and cooling processes at 65 °C and 25 °C. These evidencesn implied that the negative thermoelectric behavior was likely to have generality for halide anions, in Cu^{2+} inorganic electrolytes.

By adjusting the concentration of $CuCl_2$, we further discussed the thermopower of PVA-cellulosic membrane infiltrated by the $CuCl_2$-PEO aqueous solution. With the increase of $CuCl_2$ concentration, the absolute thermopowers of the samples first increased and then decreased in the negative thermopower direction (Fig. 4e, Supplementary Figs. 21 and 22). The maximum thermopower was -26.250 mV·K^{-1} and it occurred at the $CuCl_2$ concentration of 0.8 mol/L, which was one of the best n-type ionic thermoelectric materials under the same conditions (Fig. 4f and Supplementary Table 2). The increase of $CuCl_2$ concentration promoted more Cu^{2+} coordination interaction with PEO or PVA-cellulosic membrane, and then formed a rich environment for chloride ions. It finally led to the synthesis of $[CuCl_4]^{2-}$ with higher ion transport heat. But higher concentrations of $CuCl_2$ ($\geq$1.0 mol/L) will also inevitably led to the shielding of ion-polymer interactions by the salt ions, and the thermal mobilities of ions tended to converge to the $CuCl_2$ aqueous solutions[21,47].

The ionic conductivity measurements showed that the conductivity of the $CuCl_2$-PEO aqueous solution was higher than that of the infiltrated PVA-cellulosic membrane (Fig. 4g and Supplementary Fig. 23). This can be attributed to the strong coordination binding of Cu^{2+} by the cellulosic membrane. Moreover, the ionic conductivity of the PVA-cellulosic membrane infiltrated with 0.8 mol/L $CuCl_2$-PEO was 8.47 mS·cm^{-1}, while the thermal conductivity was also as low as 0.466 W·m^{-1}·K^{-1}. These devices also exhibited a near-ideal rectangular shape in the typical cyclic voltammetry test curves and the symmetrical constant current charge-discharge curves, which represented purely capacitive behavior (Fig. 4h and Supplementary Fig. 24).

Ionic thermoelectric capacitors (i-TE)

Before evaluating the thermal charging behavior of ionic conductors, it must be stated that, in contrast to the electronic conductors, ions cannot pass through the electrode/electrolyte interface to external circuits[10,20,22,23]. The thermal charging behavior of ionic conductors is generally based on thermal diffusion capacitor theory. We sandwiched the PVA-cellulosic membrane infiltrated by PEO aqueous solution of 0.8 mol/L $CuCl_2$ between two Pt electrodes and exposed to a temperature difference of 4.6 K. The charge-discharge behavior of PVA-cellulosic membrane can be divided into four stages (Fig. 5c). In the first stage, the i-TE device was exposed to a temperature gradient, which led to the accumulation of anions ($[CuCl_4]^{2-}$) on the cold side to generate a thermovoltage. The PVA-cellulosic membrane can achieve a stable thermal voltage of -121.464 mV during the charging stage in 30 min (Fig. 5a). In the second stage, when an external load resistor was connected to the i-TE device, the electrons and holes in the external circuit would spontaneously compensate for the voltage change caused by the thermal motion of the ions. The non-zero voltage drop of this stage was related to the electron leakage current, which can further lead to undesired self-discharge phenomenon[10]. In addition, the discharge time gradually became longer as the external load resistance increased (Fig. 5b and Supplementary Fig. 25). In the third stage, when the external load resistance and temperature gradient were removed, the anions and cations accumulated on both sides of the electrodes returned to their original state. And because the external circuit was disconnected, the electrons remained on the electrodes and created a reverse voltage. During this process, there was usually a charge transfer between the PVA-cellulosic membrane and the electrodes. Therefore, the absolute thermoelectric potential increasing in the third stage was
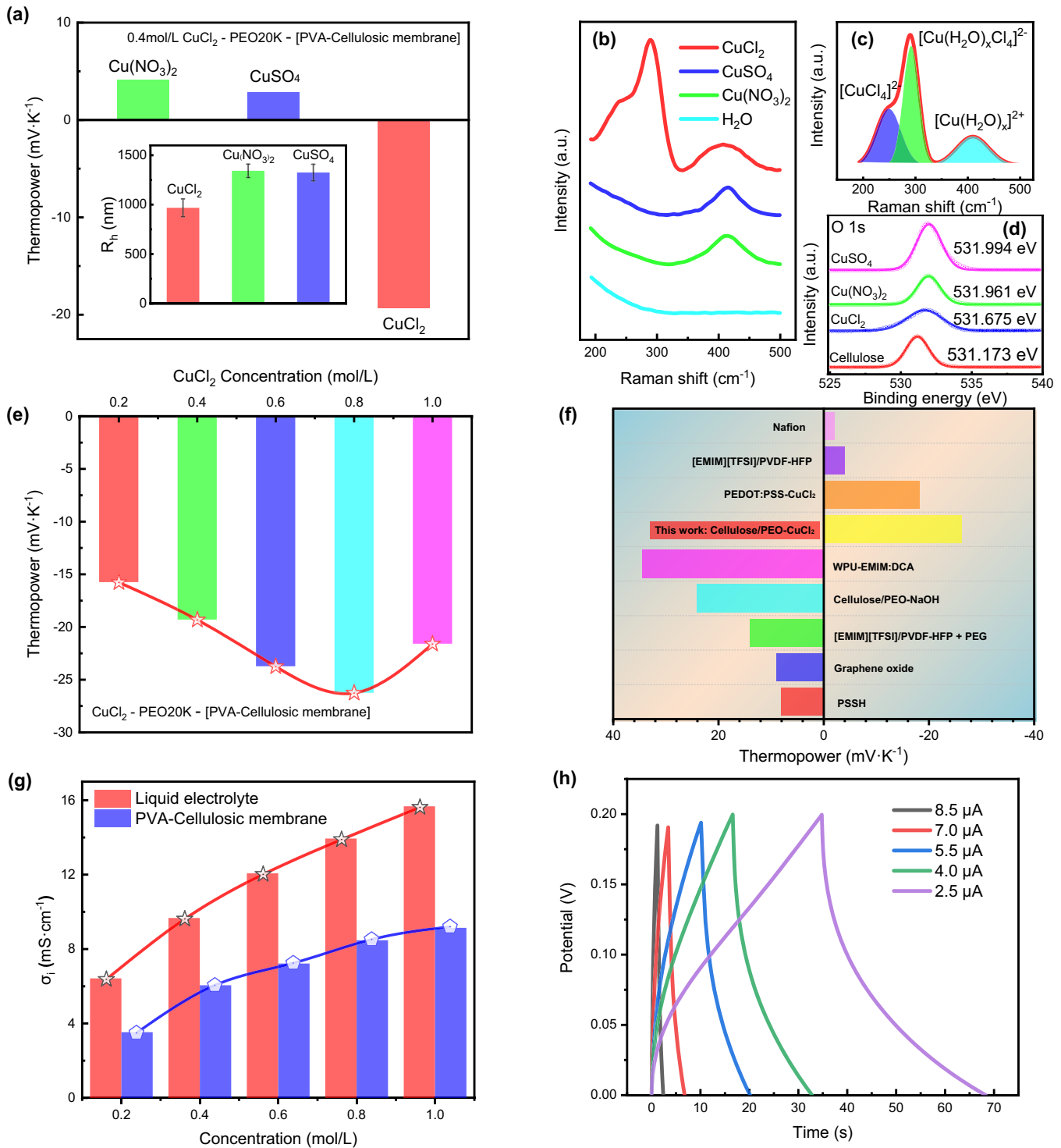
Fig. 4 Ion transport and regulation capabilities of PVA-cellulosic membranes. a Measured thermopowers of PVA-cellulosic membrane infiltrated with PEO aqueous solution of 0.4 mol/L $Cu(NO_3)_2$, $CuSO_4$ and $CuCl_2$. Hydrodynamic radius of $Cu(NO_3)_2$-cellulose, $CuSO_4$-cellulose and $CuCl_2$-cellulose aqueous solutions were shown in the inset. **b** The Raman peaks representing Cu^{2+} solvation configurations of saturated $Cu(NO_3)_2$, $CuSO_4$ and $CuCl_2$ aqueous solution. **c)** The fitted peaks of saturated $CuCl_2$ aqueous solution. **d** High-resolution O 1 s photoelectron spectra of the $Cu(NO_3)_2$-[PVA-cellulosic membrane], $CuSO_4$-[PVA-cellulosic membrane] and $CuCl_2$-[PVA-cellulosic membrane]. **e** Thermopowers of PVA-cellulosic membranes infiltrated by the $CuCl_2$-PEO aqueous solution of different $CuCl_2$ concentration. **f** Thermopowers of the various i-TE materials (Supplementary Table 2). **g** The ionic conductivity of PVA-cellulosic membrane measured at different $CuCl_2$ concentrations. **h** The constant current charge-discharge curves of the PVA-cellulosic membrane infiltrated with $CuCl_2$-PEO aqueous solution.
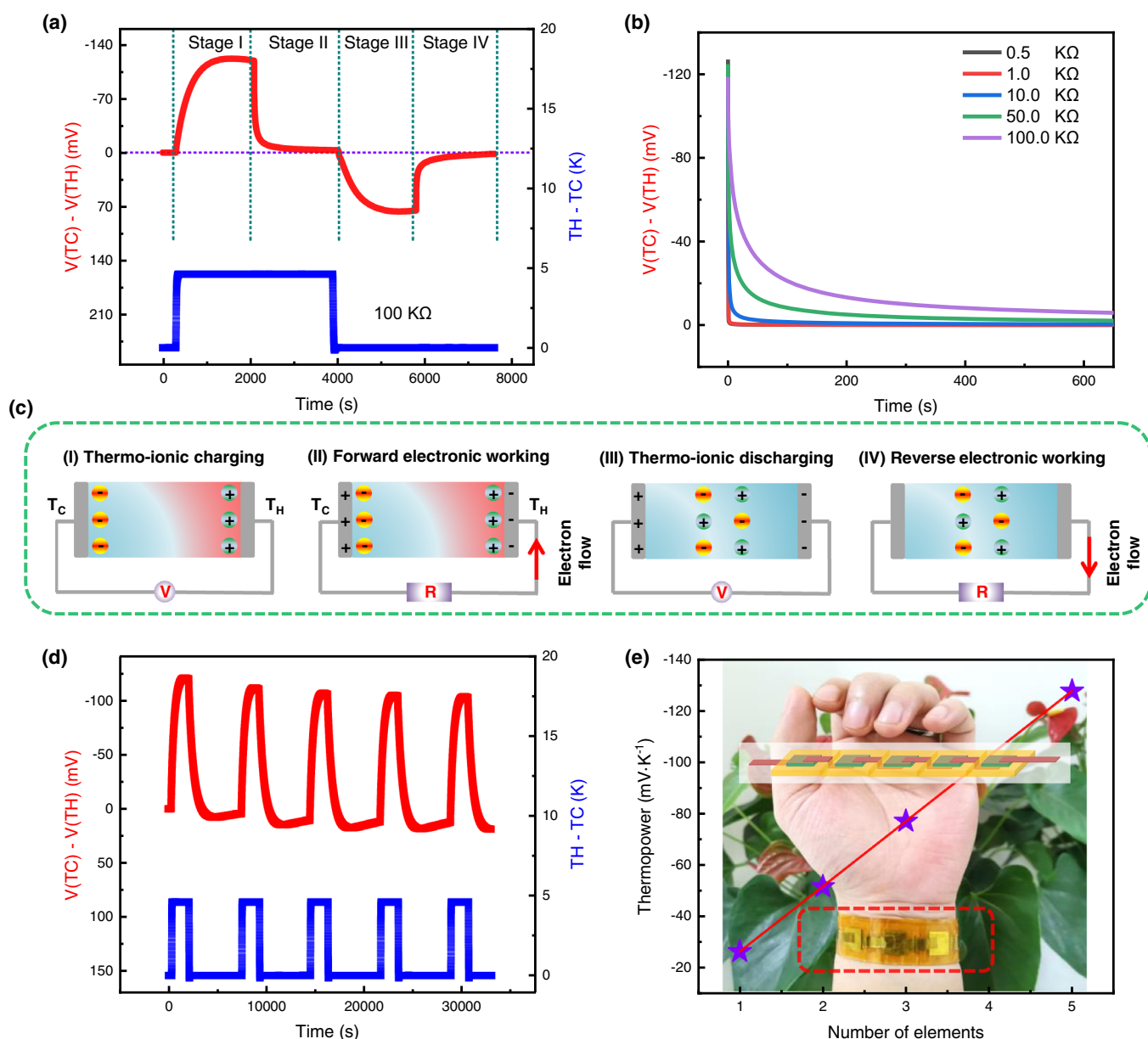
Fig. 5 Thermoelectric properties of PVA-cellulosic membranes. a The typically full thermo-ionic charging and electronic discharging cycle curve of PVA-cellulosic membrane infiltrated with 0.8 mol/L CuCl₂-PEO aqueous solution. **b** Voltage decay curves on the external load with different resistances connected to the i-TE during stage II. **c** Illustration of the working principles for ionic thermoelectric devices. **d** Output voltage of the PVA-cellulosic membrane under 5 repeated heating-cooling cycles at the temperature difference of 4.6 K. **e** The improved thermopower of modular i-TE device. Photo credit: Bin Chen, Department of Electrical and Electronic Engineering, Southern University of Science and Technology.

generally smaller than that in the first stage. In the fourth stage, when the external load was reconnected, the electrons gathered on the electrodes flowed out and the voltage on the external load dropped to zero.

We also repeatedly obtained the thermal response voltage of the i-TE device for 5 thermal charging and cooling processes (Fig. 5d). This was important for the repeated use of thermoelectric capacitors. Finally, the application scenes of our designed i-TE devices were mainly oriented in the field of self-functioning wearable thermoelectric devices. Although, limited by the power of our temperature control system, we only characterized the thermal response behavior in the 4.6 K temperature range. At the room temperature of 27 °C, the temperature difference between the human body and the external environment is 3–8 K (Supplementary Fig. 26), and our i-TE device can be well used[48].

For example, through the assembly of five modular i-TE devices, it can be easily worn as an energy bracelet (Fig. 5e). Using the standardized thermoelectric test system, the wristband achieved a maximum thermopower of −127.827 mV·K⁻¹.

In summary, we have demonstrated a giant negative thermoelectric property in the PVA-cellulosic membranes infiltrated by PEO aqueous solutions of CuCl₂, which depends on copper-coordinated PEO and carboxylated cellulose. By optimizing the concentration of CuCl₂, high thermopower ranging from −15.75 to −26.25 mV·K⁻¹ was achieved. We proved the importance of the synthesized $[CuCl_4]^{2-}$ complexes of Cu^{2+} and Cl^- in the n-type ionic thermoelectric material design. Moreover, the PVA-cellulosic membrane also has a higher ionic conductivity of 8.47 mS·cm⁻¹ and a lower thermal conductivity of 0.466 W·m⁻¹·K⁻¹. This cellulosic membrane-based ionic conductor holds broad promise

for large-scale energy harvesting, sustainable thermal conversion of energy, and wearable technology.

METHODS

Materials

Carboxylated cellulose (4–10 nm in diameter, 200 nm in length), uncarboxylated cellulose (25 μm), PEO20K, polyvinyl alcohol PVA (molecular weight, 146,000 to 186,000; 98–99% hydrolyzed), $Cu(NO_3)_2$, $CuSO_4$, $CuCl_2$, $CuBr_2$, $NaCl$, $MgCl_2$, $AlCl_3$, $CaCl_2$, $FeCl_3$, $CoCl_2$, $ZnCl_2$, NaOH and HCl were purchased from Shanghai Macklin Biochemical Technology Co., Ltd. Deionized water was purified using Milli-Q Direct 8 ultrapure water system (Millipore, Billerica, MA), with a minimum resistivity of 18.2 MΩ·cm. All chemicals were used without further purification.

Preparation of the PVA-cellulosic membrane

All of our PVA-cellulosic membranes were first synthesized from 1 wt% carboxylated cellulose and 5 wt% polyvinyl alcohol aqueous solution. The aqueous solution was heated and stirred in a water bath at 100 °C for 24 h. Then, the PVA-cellulose solution was defoamed and poured into a mold, frozen at −20 °C for 12 h, and thawed at 25 °C for 12 h to prepare a freeze-thawed PVA-cellulose hydrogel. Next, we washed the hydrogel by repeated soaking in the deionized water with changing the water every 30 min and for a total of 6 h. Finally, we frozen the deionized water-purified hydrogels in a refrigerator for 24 h and obtained the PVA-cellulosic membranes through a freeze-drying process of 3 days (FD-1A-50 +, BIOCOOL). Moreover, for the preparation of pure PVA membrane and PVA-cellulosic membrane (without COO⁻ group), except replacing carboxylated cellulose with PVA or cellulose of the same quality, the other preparation processes refer to the preparation method of PVA-cellulosic membrane.

Infiltration of PVA-cellulosic membrane

The polymer aqueous solution of 35 wt% PEO (20 K) and 65 wt% deionized water were stirred until completely dissolved. Then added different concentrations of $CuCl_2$ (0.2–1.0 mol/L, the $CuCl_2$ concentration relative to deionized water) and stirred until the $CuCl_2$ particles are completely dissolved. The PVA-cellulosic membrane was infiltrated in a container containing the prepared polymer electrolyte and placed the container into a vacuum infiltration chamber (50 KPa). Visible air bubbles can be seen in the liquid until the PVA-cellulose membrane was fully penetrated. Finally, the PVA-cellulosic membrane was taken out from the polymer electrolyte.

Fabrication of the i-TE module

A layer of dielectric elastomer (3M-VHB4905) was cut into a square plate with a square hole (the size of $8 \times 8 \times 2$ mm) at the center using a laser cutter (UNIVERSAL), followed by laminating onto one layer Pt electrode. Then the PVA-cellulosic membrane infiltrated with polymer electrolyte was added into the square hole. Finally, we laminated another Pt electrode to the other side of the VHB tape. In addition, we also chose Ti foil as the current collector and encapsulated with polyimide tape on the outermost layers of the device.

Characterization of chemical properties

The hydrodynamic radius (R_h) and zeta potential of $CuCl_2$ nanoparticles in suspension were measured using dynamic light scattering (DLS) spectra with a Malvern Zetasizer Nano ZS90. The instrument operated at a wavelength of 633 nm, a scattering angle of 173 and a temperature of 25 °C. The refractive index of the dispersant and the viscosity of water were taken to be 1.330

and 0.8872 cP, respectively. Then, 60 μl of an $CuCl_2$-cellulose and $CuCl_2$-PEO aqueous solutions were respectively mixed with 5 ml and 100 ml of deionized water for dilution. A supernatant solution was stabilized in a cuvette for 3 h. Error bars reflect the standard deviation from three identical measurements. X-ray photoelectron spectroscopy (XPS) analysis was conducted on a PHI 5000 Versaprobe II pectrometer. All the spectra were calibrated to the binding energy of the adventitious C1s peak at 284.8 eV. Raman spectroscopies for the aqueous electrolyte solution and PVA-cellulosic membrane were conducted on Horiba LabRAM HR Evolution microscope by using a 532 nm excitation laser.

Characterization of electrochemical properties

Rex DDS 11 A ionic conductivity meter was used to measure the ionic conductivity of polymer electrolyte aqueous solution and the PVA-cellulosic membrane infiltrated with $CuCl_2$-PEO aqueous solution at 25 °C. The conductivity meter was equipped with a DJS-1C platinum black conductivity electrode (the electrode constant was 0.988). The cyclic voltammetry (CV) curves in the range of 0–0.2 V and the constant current charge-discharge curve were measured by an electrochemical workstation (Shanghai Chenhua Instrument Co. Ltd., CHI660E).

Thermal conductivity measurement

Laser flasher was widely used to measure the transient thermal conductivity of solid and liquid materials[20]. The formula for thermal conductivity measurement can be expressed as $k = a\rho C_p$. Among them, k is thermal conductivity, a is thermal diffusivity, ρ is density and C_p is heat capacity. For the PVA-cellulosic membrane infiltrated with 0.8 mol/L $CuCl_2$-PEO aqueous solution, the thermal diffusivity measured by the NETZSCH LFA 457 MicroFlash™ laser thermal conductivity meter was 0.141 mm²·s⁻¹. The density of PVA-cellulosic membrane was 2.25 g·cm⁻³. And the heat capacity measured by the differential scanning calorimeter (NETZSCH-DSC204F1 Phoenix) was 1.47 J·g⁻¹·K⁻¹. We thus calculated the thermal conductivity to be 0.466 W·m⁻¹·K⁻¹.

Characterization of thermopower

The thermopower and temperature gradient (1.5, 3.1 and 4.6 K) was determined from a homemade setup using an Keithley 2400 voltmeter, and the TEC temperature control module TCM-X107 purchased from China's Sichuan Yexian Technology, respectively. The temperature sensitivity of the temperature control module was 0.002 °C. For the general measurement, two Peltier devices attached to an aluminum heat sink linked by a thermal paste were used to generate the temperature gradient. In addition, we further used ultra-fine K-type thermocouples for the second temperature calibration to ensure the authenticity and accuracy of the temperature.

Theoretical calculation of thermopower

Theoretical calculation of thermopower for the salt ion in dilute aqueous solution was according to the Agar model based on the Born theory[15–17]. Thermal diffusion of ions under a temperature gradient creates an ionic charge gradient, which results in a potential gradient. The thermally induced ion flow for each moving ion can be expressed as:

$$J_{\pm} = -D_{\pm}\left(\nabla n_{\pm} + 2n_{\pm}a_{\pm}\frac{\nabla T}{T} \mp n_{\pm}\frac{eE}{k_B T}\right) \qquad (1)$$

$J_{\pm}$ is the thermally induced ion current by per mobile ion; $D_{\pm}$ is the ionic self-diffusion coefficient; $n_{\pm}$ is ion density.

Assuming steady-state conditions ($J_{\pm} = 0$) and zero net charge conditions ($\nabla n_+ - \nabla n_- = 0$) in an electrolyte containing positive and negative ions, the thermopower (S) of thermal diffusion of

ions can be expressed as:

$$S = (a_+ - a_-)(k_B/e) \tag{2}$$

where a is the Soret coefficient of the ionic specie in the dilute aqueous solution, k_B is the Boltzmann constant (1.380649×10^{-23} J·K^{-1}) and e is the electron charge ($1.602176634 \times 10^{-19}$ C = $1.602176634 \times 10^{-19}$ J·V^{-1}).

According to the agar Agar model, the ionic Soret coefficient can be calculated by the following formula:

$$a = \frac{Q^*}{2k_BT} = Q^{*\underline{O}}N_A/(2k_BT) = Q^{*\underline{O}}/(2RT) \tag{3}$$

$Q^{*\underline{O}}$ is the standard single ion transport heat[14,17], R is the ideal gas constant (8.314 J·mol^{-1}·K^{-1}), N_A is the Avogadro number (6.02×10^{23} mol^{-1}) and T is the actual calculated temperature (300 K).

DATA AVAILABILITY

The data that support the findings of this study are available from the corresponding authors upon reasonable request.

REFERENCES

1. Jia, Y. et al. Wearable thermoelectric materials and devices for self-powered electronic systems. *Adv. Mater.* **33**, 2102990 (2021).
2. Kim, S. J., We, J. H. & Cho, B. J. A wearable thermoelectric generator fabricated on a glass fabric. *Energy Environ. Sci.* **7**, 1959–1965 (2014).
3. Kim, S. J. et al. High-performance flexible thermoelectric power generator using laser multiscanning lift-off process. *ACS Nano* **10**, 10851–10857 (2016).
4. Du, C. et al. Toward precision recognition of complex hand motions: wearable thermoelectrics by synergistic 2D nanostructure confinement and controlled reduction. *Adv. Funct. Mater.* **32**, 2206083 (2022).
5. Liang, L. et al. Initiating a stretchable, compressible, and wearable thermoelectric generator by a spiral architecture with ternary nanocomposites for efficient heat harvesting. *Adv. Funct. Mater.* **32**, 2111435 (2022).
6. Li, Z. et al. Mechanically robust and flexible films of ionic liquid-modulated polymer thermoelectric composites. *Adv. Funct. Mater.* **31**, 2104836 (2021).
7. Lv, H. et al. A flexible spring-shaped architecture with optimized thermal design for wearable thermoelectric energy harvesting. *Nano Energy* **88**, 106260 (2021).
8. Chang, C. et al. 3D charge and 2D phonon transports leading to high out-of-plane ZT in n-type SnSe crystals. *Science* **360**, 778–783 (2018).
9. Jiang, B. et al. High-entropy-stabilized chalcogenides with high thermoelectric performance. *Science* **371**, 830–834 (2021).
10. Zhao, D. et al. Ionic thermoelectric supercapacitors. *Energy Environ. Sci.* **9**, 1450–1457 (2016).
11. Liu, S. et al. Giant and bidirectionally tunable thermopower in nonaqueous ionogels enabled by selective ion doping. *Sci. Adv.* **8**, eabj3019 (2022).
12. Chi, C. et al. Selectively tuning ionic thermopower in all-solid-state flexible polymer composites for thermal sensing. *Nat. Commun.* **13**, 1–10 (2022).
13. Chen, B. et al. Giant negative thermopower of ionic hydrogel by synergistic coordination and hydration interactions. *Sci. Adv.* **7**, eabi7233 (2021).
14. Liu, K. et al. Flexible and robust bacterial cellulose-based ionogels with high thermoelectric properties for low-grade heat harvesting. *Adv. Funct. Mater.* **32**, 2107105 (2022).
15. Agar, J. N., Mou, C. Y. & Lin, J. L. Single-ion heat of transport in electrolyte solutions: a hydrodynamic theory. *J. Phys. Chem.* **93**, 2079–2082 (1989).
16. Kim, S. L., Hsu, J. H. & Yu, C. Thermoelectric effects in solid-state polyelectrolytes. *Org. Electron.* **54**, 231–236 (2018).
17. Takeyama, N. & Nakashima, K. Proportionality of intrinsic heat of transport to standard entropy of hydration for aqueous ions. *J. Solut. Chem.* **17**, 305–325 (1988).
18. Cheng, H., He, X., Fan, Z. & Ouyang, J. Flexible quasi-solid state ionogels with remarkable seebeck coefficient and high thermoelectric properties. *Adv. Energy Mater.* **9**, 1901085 (2019).
19. Chikina, I., Shikin, V. & Varlamov, A. A. Seebeck effect in electrolytes. *Phys. Rev. E* **86**, 011505 (2012).
20. Li, T. et al. Cellulose ionic conductors with high differential thermal voltage for low-grade heat harvesting. *Nat. Mater.* **18**, 608–613 (2019).
21. Han, C. G. et al. Giant thermopower of ionic gelatin near room temperature. *Science* **368**, 1091–1098 (2020).
22. Kim, B. et al. Robust high thermoelectric harvesting under a self-humidifying bilayer of metal organic framework and hydrogel layer. *Adv. Funct. Mater.* **29**, 1807549 (2019).
23. Kim, B., Hwang, J. U. & Kim, E. Chloride transport in conductive polymer films for an n-type thermoelectric platform. *Energy Environ. Sci.* **13**, 859–867 (2020).
24. Zhang, Q. et al. Modulating electrolyte structure for ultralow temperature aqueous zinc batteries. *Nat. Commun.* **11**, 1–10 (2020).
25. Li, Y. et al. Li$^+$ selectivity of carboxylate graphene nanopores inspired by electric field and nanoconfinement. *Small* **17**, 2006704 (2021).
26. Li, Y. Y. et al. Distinctive hydration dynamics around highly coordinated Cu^{2+}/Zn^{2+}-chloride complexes: a molecular dynamics simulation study. *J. Mol. Liq.* **314**, 113619 (2020).
27. Ogawa, Y. et al. Formation and stability of cellulose-copper-NaOH crystalline complex. *Cellulose* **21**, 999–1006 (2014).
28. Yang, C. et al. Copper-coordinated cellulose ion conductors for solid-state batteries. *Nature* **598**, 590–596 (2021).
29. Ke, H. et al. Shear-induced assembly of a transient yet highly stretchable hydrogel based on pseudopolyrotaxanes. *Nat. Chem.* **11**, 470–477 (2019).
30. Savoie, B. M., Webb, M. A., IIIThomas, F. & Miller. Enhancing cation diffusion and suppressing anion diffusion via Lewis-acidic polymer electrolytes. *J. Phys. Chem. Lett.* **8**, 641–646 (2017).
31. Cao, L. et al. Solvation structure design for aqueous Zn metal batteries. *J. Am. Chem. Soc.* **142**, 21404–21409 (2020).
32. Kim, C. S. & Oh, S. M. Importance of donor number in determining solvating ability of polymers and transport properties in gel-type polymer electrolytes. *Electrochim. Acta* **45**, 2101–2109 (2000).
33. Gutmann, V. Solvent effects on the reactivities of organometallic compounds. *Coord. Chem. Rev.* **18**, 225–255 (1976).
34. Kong, W. et al. Muscle-inspired highly anisotropic, strong, ion-conductive hydrogels. *Adv. Mater.* **30**, 1801934 (2018).
35. Wang, R. et al. Holistically engineered polymer-polymer and polymer-ion interactions in biocompatible polyvinyl alcohol blends for high-performance triboelectric devices in self-powered wearable cardiovascular monitorings. *Adv. Mater.* **32**, 2002878 (2020).
36. Qin, H. et al. Multifunctional superelastic cellulose nanofibrils aerogel by dual ice-templating assembly. *Adv. Funct. Mater.* **31**, 2106269 (2021).
37. Darabi, M. A. et al. An alkaline based method for generating crystalline, strong, and shape memory polyvinyl alcohol biomaterials. *Adv. Sci.* **7**, 1902740 (2020).
38. Yu, B. et al. Thermosensitive crystallization-boosted liquid thermocells for low-grade heat harvesting. *Science* **370**, 342–346 (2020).
39. Lim, H., Shi, Y., Wang, M. & Qiao, Y. Effects of work function on thermal sensitivity of electrode potential. *Appl. Phys. Lett.* **106**, 223901 (2015).
40. Horike, S. et al. Outstanding electrode dependent Seebeck coefficients in ionic hydrogels for thermally chargeable supercapacitor near room temperature. *ACS Appl. Mater. Inter.* **12**, 43674–43683 (2020).
41. Würger, A. Thermopower of ionic conductors and ionic capacitors. *Phys. Rev. Res.* **2**, 042030 (2020).
42. Würger, A. Thermoelectric ratchet effect for charge carriers with hopping dynamics. *Phys. Rev. Lett.* **126**, 068001 (2021).
43. Manning, G. S. Limiting laws and counterion condensation in polyelectrolyte solutions. 8. Mixtures of counterions, species selectivity, and valence selectivity. *J. Phys. Chem.* **88**, 6654–6661 (1984).
44. Zhang, C. et al. A ZnCl$_2$ water-in-salt electrolyte for a reversible Zn metal anode. *Chem. Commun.* **54**, 14097–14099 (2018).
45. Chastain, J. & King Jr, R. C. Handbook of X-ray Photoelectron Spectroscopy (Perkin-Elmer, 1992).
46. Waizumi, K., Masuda, H., Einaga, H. & Fukushima, N. Intrinsic structures of [CuCl$_4$]$^{2-}$ and [CuBr$_4$]$^{2-}$ anions by Ab initio density functional calculations. *Chem. Lett.* **22**, 1145–1148 (1993).
47. Tobias, D. J. & Hemminger, J. C. Getting specific about specific ion effects. *Science* **319**, 1197–1198 (2008).
48. Webb, P. Temperatures of skin, subcutaneous tissue, muscle and core in resting men in cold, comfortable and hot conditions. *Eur. J. Appl. Physiol.* **64**, 471–476 (1992).

AUTHOR CONTRIBUTIONS

B.C., J.F. and Q.C. contributed equally to this work. B.C. and T.W. designed the experiment, B.C., J.F., Q.C., S.X., J.Y., X.Z. and Z.L. conducted the experiment. B.C., J.F. and Q.C. performed DLS, XPS, and Raman measurements. B.C., T.W., J.F. and Q.C. performed the theoretical derivation to explain the experimental data. B.C. and T.W. wrote the manuscript. All authors discussed the results and participated in the final review of the manuscript.

COMPETING INTERESTS

The authors declare no competing interests.

ADDITIONAL INFORMATION

Supplementary information The online version contains supplementary material available at https://doi.org/10.1038/s41528-022-00213-4.

Correspondence and requests for materials should be addressed to Taihong Wang.

Reprints and permission information is available at http://www.nature.com/reprints

Publisher's note Springer Nature remains neutral with regard to jurisdictional claims in published maps and institutional affiliations.